creative commons
COMMONS DEED

저작자표시-비영리-변경금지 2.0 대한민국

이용자는 아래의 조건을 따르는 경우에 한하여 자유롭게

- 이 저작물을 복제, 배포, 전송, 전시, 공연 및 방송할 수 있습니다.

다음과 같은 조건을 따라야 합니다:

저작자표시. 귀하는 원저작자를 표시하여야 합니다.

비영리. 귀하는 이 저작물을 영리 목적으로 이용할 수 없습니다.

변경금지. 귀하는 이 저작물을 개작, 변형 또는 가공할 수 없습니다.

- 귀하는, 이 저작물의 재이용이나 배포의 경우, 이 저작물에 적용된 이용허락조건을 명확하게 나타내어야 합니다.
- 저작권자로부터 별도의 허가를 받으면 이러한 조건들은 적용되지 않습니다.

저작권법에 따른 이용자의 권리는 위의 내용에 의하여 영향을 받지 않습니다.

이것은 이용허락규약(Legal Code)을 이해하기 쉽게 요약한 것입니다.

Disclaimer

dCollection

이학박사 학위논문

Mechanistic study on Complexin using magnetic tweezer

자기집개를 이용한 Complexin에 대한 연구

2021년 8월

서울대학교 대학원

자연과학대학 생명과학부

김 해 수

Mechanistic study on Complexin using magnetic tweezer

지도교수 윤 태 영

이 논문을 이학박사 학위논문으로 제출함
2021년 5월

서울대학교 대학원
자연과학대학 생명과학부
김 해 수

김해수의 박사 학위논문을 인준함
2021년 5월

위 원 장 _____

부위원장 _____

위 원 _____

위 원 _____

위 원 _____

국문초록

SNARE 복합체는 시냅스 전 막과의 시냅스 소포 융합을 촉매합니다. Complexin (Cpx)은 SNARE에 단단히 결합하고 막 융합을 조절하는 presynaptic 단백질입니다. 하지만 Cpx 가 SNARE 복합체에 힘이 가해진 상태에서 SNARE 복합체의 에너지 경관을 어떻게 조절하는지는 알려져 있지 않습니다.

본 연구에서는 Cpx가 자기 집개를 사용하여 단일 SNARE 복합체와 어떻게 상호 작용하는지를 보여줍니다. 놀랍게도 Cpx의 효과는 13pN 이상의 높은 기계적 장력에서만 볼 수 있습니다. Cpx는 SNARE의 중앙 부분을 안정화하는 동시에 링커 도메인 결합을 억제하여 SNARE의 완전한 접힘을 방지합니다.

즉 링커가 열린 형태에서 Cpx이 뉴런 SNARE 복합체에 대한 직접적인 멈춤작용 효과를 나타냅니다. 이러한 발견은 Cpx 및 신경 SNARE가 동시다발적 신경 전달 물질 방출을 준비하기 위해 Cpx 가 시냅스 소포체와 함께 작동함을 시사합니다.

.....

주요어 : 자기집게, 컴플렉신, 스네어 복합체, 신경전달, 힘 스펙트로스코피, 신경과학

학 번 : 2017-36517

목 차

Introduction

Synaptic vesicle exocytosis is tightly controlled to allow for efficient neurotransmission. As calcium influx occurs, a pool of vesicles docked to the presynaptic plasma membrane fuse with the membrane, eliciting rapid synchronous neurotransmitter release[1]. The zippering of neuronal soluble N-ethylmaleimide-sensitive factor attachment protein receptor (SNARE) proteins provides the large energy needed to overcome the energy barrier against fusion, making SNARE complexes the heart of the membrane fusion machinery[2]. Furthermore, regulatory proteins such as complexin (Cpx) and synaptotagmin provide critical control points by inhibiting fusion during the resting phase and completing it quickly within a millisecond when activated[3] Cpx is the only presynaptic protein known to stably bind to the neuronal SNARE complex[4], implying that it can regulate neuronal SNARE assembly directly. In the past two decades, research into the role of Cpx in neurotransmission has produced a number of suggestions as to its function ((see refs. [5,6] for recent reviews). The different effects of Cpx on evoked and spontaneous synaptic vesicle releases made it difficult to interpret some of the early experimental findings[5,7]. Cpx promotes Ca2+-triggered release8, but prevents spontaneous fusion9,10. For instance, experimental results with invertebrates such as the Drosophila neuromuscular junction illustrate the Cpx's spontaneous fusion clamping

effect[10], which is attributed to the highly charged accessory helix of the Drosophila Cpx [11]. When mammalian Cpx, which has less charges on the accessory helix, replaces endogenous Cpxs in Drosophila, the clamping effect is reduced[12,13]. Because of the contradictory preparations of truncated Cpx variants and SNARE proteins, as well as the various biological structures used across experiments, the mechanistic aspects of how Cpx affects a SNARE complex remain a mystery[11,14-16]. The way Cpx's multiple domains interact with the SNARE complex is thought to be the cause of its effects[17,18]. Short helical domains and unstructured regions make up Cpx, a short linear protein. Cpx's central helix is primarily responsible for the protein's strong binding to the neuronal SNARE complex[19-21], and its presence is needed to observe nearly all of Cpx's known impact. The accessory helix and N-terminal domain both interact with neuronal SNAREs, affecting vesicle fusion in disparate ways. It has been reported that the N-terminal domain, which may form a short amphipathic helix, interacts with both the SNARE complex and the plasma membrane, promoting fusion in general[17,22-24]. The accessory helix, on the other hand, has often been hypothesized to interact with SNARE complex assembly and prevent fusion[22,25-28]. Finally, Cpx's C-terminal domain is less structured than the helical segments and has been confirmed to direct synaptic vesicles to fusion sites[29,30]. However, in a physiological environment, all of Cpx's domains will cooperate together, necessitating a comprehensive understanding of the protein's function.

Furthermore, no one has looked into how mechanical tension in neuronal SNARE complexes affects the observed effects of Cpx. Because of electrostatic repulsion, hydration barrier, and steric hindrance between the two fusing membranes, tension rapidly builds up when a synaptic vesicle contacts a presynaptic membrane[31,32]. The energy landscape that regulates SNARE zippering processes has been shown to be dramatically shifted by this stress in a SNARE complex[33,34]. Mechanical stress can also drastically alter the subsequent interactions between Cpx and SNAREs. Unfortunately, how the different sections of Cpx interact on a single SNARE complex under such force-loaded conditions is unknown. Although Cpx has been proposed to clamp partially zippered SNARE complexes and thus prevent membrane fusion[21,25-28], it has proven difficult to observe such an intermediate conformation of the neuronal SNARE complex in the absence of applied stress, possibly due to the transient existence of this state. Here, we investigated how mammalian Cpx regulates the conformation of the neuronal SNARE complex under mechanical tension. We directly observed the rapid transition between intermediate conformations of single neuronal SNARE complexes when applying 12 - 16 pN of tension with magnetic tweezers. By adding Cpx to the mechanical unzipping and rezipping cycles of the pre-assembled SNARE complexes, we have discovered that Cpx significantly stabilizes the assembled SNARE complexes. Cpx also prevents the SNARE complex from completely zippering by interfering with the assembly of the SNARE linker domains. The

central-accessory helices and the N-terminal domain of Cpx, respectively, mediate the stabilizing and inhibitory effects. All in all, Cpx's two effects work together to facilitate the SNARE complex's "linker-open" state, which clamps it in a centered, partially zippered conformation. Both of Cpx's molecular effects appear in a narrow range of applied forces, notably 13 - 16 pN, meaning that Cpx is naturally tuned to operate under a well-defined range of mechanical tensions applied to individual SNARE complexes.

Methods

Expression of recombinant proteins. For the SNARE proteins used in this study, 6×His-tagged rat syntaxin-1A (191 - 268, I202C/K266C), rat SNAP-25 isoform b (2 - 206, C85A/C88A/C90A/C92A), and rat synaptobrevin-2 (2 - 97, L32C/I97C) were cloned into pET28a vector. Rat Cpx-1 variants (1 - 134, 1 - 80, 32 - 80, and 48 - 73) were cloned into HRV 3C cleavage site-inserted pGEX-4T-1 vector. The difference between rat and human proteins in the region we studied are (rat/ human): none in syntaxin-1A and SNAP-25b; V8/A in synaptobrevin-2; V61/A, M62/V, P109/V, F132/L (the former two in the central helix and the latter two in the C-terminal domain) in Cpx-1. All proteins were expressed in E. coli Rosetta (DE3) pLysS strain (Novagen). For Cpx, cells were grown in Luria - Bertani broth (LB) with 100 $\mu g ml^{-1}$ ampicillin and 34 $\mu g ml^{-1}$ chloramphenicol. For expressing SNARE

proteins, 25 μgml^{-1} kanamycin was used instead of ampicillin. Bacteria in 25 ml LB overnight culture (37 °C, 220 r.p.m.) were transferred into the main culture. Cells were grown (37 °C, 220 r.p.m.) to an optical density of 0.7 - 0.8 (600 nm) and 0.5 mM isopropyl-β-D-1-thiogalactoside (IPTG) was added to induce expression. After further incubation for 3 - 4 h (37 °C, 220 rpm), cells were cen- trifuged at 5000×g for 10 min Harvested cell pellets were frozen with liquid nitrogen and stored at −80 °C.

Purification of recombinant proteins. Buffers used for protein purification are listed in Supplementary Note 1. Cell pellets expressing recombinant proteins were thawed at room temperature, suspended in 30 ml of ice-cold lysis buffer, and broken up by sonication on ice. Lysates were centrifuged at 15,000 × g for 30 min at 4 °C to remove insoluble materials. Then, the supernatant was bound to either 1 ml of GST - agarose resin (Incospharm) or nickel agarose resin (Qiagen). Bound resins were poured into a gravity column and washed with 100 ml of wash buffer, and the bound proteins were eluted with elution buffer. For Cpxs, HRV-3C protease supplemented to cleave the target proteins from GST (4 °C, 90 min) in the elution buffer. Full-length Cpx (1 - 134) were loaded onto a Superdex 200 Increase column pre-equilibrated with elution buffer for further purification. The peak fractions were collected and concentrated (Amicon Ultra 10K, Merck). Other Cpx fragments were further purified and concentrated with proper molecular weight cut-off membrane filters. Purified proteins

were verified on 12% and 20% SDS poly-acrylamide gels for SNARE and Cpx proteins, respectively. All proteins were frozen with liquid nitrogen and stored at −80 °C until use.

Conjugation of SNARE complex to DNA. Each of the two 510-bp DNA handles was produced by polymerase chain reaction using 5′-thiol-modified and either 5′-biotin-labeled or 5′-digoxigenin-labeled primers (Bionics) (Supplementary Note 2). The products were incubated with 100 mM DTT for 12 h at 37 °C to cleave unwanted disulfide bonds. After purification using QIAGEN-tip column (Qiagen), the handles were concentrated and activated with 10mM 2,2′-dithiodipyridine (DTDP) for 12 h at 37 °C. After activation, the remaining DTDP was removed using QIAGEN-tip column and ethanol-precipitated DNA pellets were solubilized with phosphate-buffered saline (PBS, pH 7.4) at the final step. Purified handles were concentrated to 3–4 μM and stored in 4 °C. To conjugate DNA handles to the SNARE complex, each SNARE protein was first mixed at an equal molar ratio and incubated with 5 mM DTT for 3 h at 25 °C for assembly. Thrombin was added and dialyzed against PBS (containing 1 mM DTT) overnight at 4 °C to remove histidine tags. To remove excessive DTT, SNARE complexes were desalted using PBS- equilibrated PD MiniTrap G-25 column (GE Healthcare) and concentrated to 58 μM. The DTDP-activated biotin-labeled DNA handle was added to the solution of SNARE complex at a molar ratio of 1:20. The SNARE/DNA mixture was incu- bated at room temperature for 30min. Then, an excessive amount of

digoxigenin- labeled DNA handle was added to the mixture and incubated for 3 h at room temperature for complete attachment. Since we do not control the reaction speci- ficity of the two DNA handles to syntaxin-1A and synaptobrevin-2, the product was a mixture of the two kinds (i.e., biotin - syntaxin - synaptobrevin - digoxigenin and biotin - synaptobrevin - syntaxin - digoxigenin) that were indistinguishable in tweezing experiments. Samples were frozen with liquid nitrogen and stored at −80 °C.

Preparation of sample chamber for magnetic tweezers. Sample chambers for magnetic tweezers were constructed from no. 1.5 glass coverslips33,35.A flow cell was assembled with two glass coverslips passivated with polyethylene glycols (PEG) (Laysan Bio), sandwiched with a double-sided tape spacer. A fraction (1 - 5%) of the PEG molecules were modified with biotin for the surface attachment of SNARE −DNA constructs via NeutrAvidin. Sequential injection of SNARE - DNA con- jugate mixed with NeutrAvidin (Thermo Fisher), reference beads (Spherotech, 3.0 - 3.4 μm in diameter), and magnetic beads (Thermo Fisher, M270) coated with anti-digoxigenin (Sigma-Aldrich) into the flow cell yielded ~1-kbp bead - tether constructs. All measurements were performed in PBS (pH 7.4) supplemented with 2.5 μM SNAP-25 to allow refolding of SNARE in case of unfolding events at high forces. All injection and washing steps were performed with a syringe pump at flow rates of 25 - 1000 μl min−1. When using Cpx, additional buffer exchange with a solution containing 5 μM Cpx was

conducted. Full details of the sample assembly procedure are given in Supplementary Table 1.

Magnetic tweezers setup and bead tracking. The magnetic tweezers apparatus was built on an inverted microscope (Olympus). A pair of magnets (vertically aligned in opposite directions with a 1-mm gap) was placed above the stage holding a flow cell. The vertical position and rotation of the magnets were controlled by a translation stage (Physik Instrumente) and a stepper motor (Autonics), respec- tively. Beads in a flow cell were illuminated by a red superluminescent diode (QPhotonics) and imaged by a 100× oil-immersion objective (Olympus) and a high-speed CMOS camera (Mikrotron). The objective position was controlled by a piezo-controlled nano-positioner (Mad City Labs) to calibrate distances and to correct for mechanical/thermal drift. The acquired images were grabbed by a frame grabber (Active Silicon) and retrieved by a custom software written in LabVIEW (National Instruments). The three-dimensional coordinates of reference and magnetic beads were tracked in real time at 100 - 1200 Hz by a custom software written in LabVIEW66.

Force calibration and scaling. Magnetic forces were measured and calibrated as described in the literature67. Forces were estimated from the power spectral den- sities for the Brownian motions of magnetic beads perpendicular to the magnetic field, correcting for near-surface viscosity and blurring and aliasing in image acquisition68. Forces were calibrated against the

distance between magnets and imaging surface using 5.4-kbp DNA and the resulting force–magnet position data were fit with a double-exponential function69. For the measurements on SNARE complex, the average unzipping force measured in each pulling construct (SNARE–DNA–bead) without Cpx was normalized to the global average of the unzipping forces (14.4 pN) measured form multiple constructs (Supplementary Fig. 4), to minimize the bead-to-bead variation in force.

Verification of SNARE complex in force-ramp experiments. The end-to-end extension of SNARE complex was monitored in real time by tracking the bead position in z following a standard method in magnetic tweezers66. The sample specificity was first verified by checking the force–extension curves in force-ramp measurements in the range 0.1–20 pN at force loading rates of ±1 pN s−1. Only the constructs exhibiting all of the signature events of SNARE complex (unzipping at 12–16 pN, rezipping at 8–12 pN, unfolding at 15–18 pN, and refolding under 2 pN) were subjected to further investigation. The unzipping and rezipping events were identified programmatically to obtain the distribution of transition force over many cycles. When necessary, the force–extension graph was compared to the model extension for the SNARE–DNA conjugate (Supplementary Note 3).

Kinetic measurements in force-jump experiments. In force-jump experiments, magnet was moved at the maximum speed (15 mm/s) to instantaneously change the applied force. In

10 - 16 pN range, this motion leads to >50 pN/s changes in force, reaching target forces within 0.1 s. The unzipping and rezipping events were identified programmatically based on the abrupt large shifts in extension to measure the lifetimes of states at the target force. The resulting lifetimes were used to sketch the energy landscape for the unzipping/rezipping transition.

Measurements of SNARE complex conformation in high-speed force-clamp experiments. The conformational equilibrium of SNARE complex was measured by tracking the magnetic bead at 1.2 kHz for >15 s at each force (long enough to reach a thermal equilibrium), and varying the force by 0.2 pN in the range 12 - 16 pN. The resulting distribution of bead coordinates was fit to a Gaussian mixture model (using fitgmdist in MATLAB (Mathworks)) with either two or three components depending on the level of force and the presence of Cpx. The locations and equilibrium populations of the intermediate states were obtained as the means and proportions of the identified Gaussian components, respectively.

Result

1. Manipulation and observation of single SNARE complexes

During mechanical manipulation, we used magnetic tweezers to examine the conformations of single neuronal SNARE

complexes[33] (Fig. 1a,b). We pre-assembled ternary SNARE complexes con- sisting of syntaxin-1A, SNAP-25, and synaptobrevin-2, and attached two 510-bp DNA handles (Fig. 1b and Supplementary Fig. 1). After that, the DNA handles were attached to a glass surface and a magnetic bead, forming a pulling build (Fig. 1a and Supplementary Table 1). Tension was produced from the C-terminus of the SNAREs, mimicking the force-loaded environment assumed for neuronal SNARE complexes during synaptic vesicle fusion[36], because the DNA handles were attached to the C-terminal ends of synaptobrevin-2 and syntaxin-1A via two artificial cysteine residues[35] (Fig. 1a,b and Supplementary Fig. 2; transmembrane domains were truncated). We covalently connected the N-termini of synaptobrevin-2 and syntaxin-1A by adding two additional cysteines that formed a disulfide bond, allowing for multiple cycles of interrogation (Fig. 1b). During our tweezing experiments, this N-terminal knotting allowed us to study only properly folded SNARE complexes. Misfolded SNARE complexes, such as anti-parallel SNAREs, were unable to shape the disulfide crosslinking, ruptured under high mechanical stress, and were thus excluded from our study. We monitored the vertical location of the magnetic bead at 100 Hz as we varied the force applied to it by shifting the permanent magnets. This allowed us to control the conformation of a single SNARE complex.

We later added Cpx proteins to the assay via microfluidic buffer exchange to study Cpx function. The SNARE - DNA

build showed a typical force-extension curve for a 1-kbp double-stranded DNA when the magnetic force was increased at a loading rate of 1 pN s^{-1}, which was consistent with the length of the two DNA handles (510 bp each) (Fig. 1c). We noticed an abrupt upward movement of the bead of 25 nm when the tension was increased over 13 pN, indicating mechanical unzipping of the SNARE complex (Fig. 1d, black arrow). This 25nm unzipping corresponds to the complete unraveling of synaptobrevin-2 from the rest of the three-helix package made up of syntaxin-1A and SNAP-25, according to our calculations (Supplementary Fig. 3 and Supplementary Note 3). We also noticed important, reversible movements of the bead prior to the main unzipping event, meaning that the tweezed SNARE complex has intermediate states[33,37-39] (Fig. 1d, red circle). We lowered the magnetic force shortly after the unzipping event to record the force-extension curve during relaxation (Fig. 1c, d, orange traces). Backward transitions of comparable size to the unzipping case were observed (Fig. 1c, d, orange arrows). Since the force-extension curve snapped back to that observed during stretching, we reasoned that this reverse transformation represents the complete re-assembly, or "rezipping," of the SNARE complex. Rezipping forces were lower than unzipping forces, indicating mechanical hysteresis in a single SNARE complex's[33] force-extension period.

Finally, when we increased the force beyond that needed to unravel synaptobrevin-2 (>15 pN), we found a 5 nm upward movement of the bead due to the dissociation of SNAP-25 (Fig.

1c, d, transition to gray trace). The addition of 2.5 μM of free SNAP-25 proteins to the assay buffer allowed SNAP-25 to re-associate with the pulling construct in the low-pN region[34] (Fig. 1c, gray to black).

2. Cpx mechanically stabilizes neuronal SNARE complexes.

We then added 5μM full-length Cpx (rat Cpx-1) to the tweezed SNARE complex (Fig. 1c, e). The dissociation constant between Cpx and a SNARE complex is known to be 10 - 70 nM[40 - 42], 5μM, which was strong enough to bind all SNARE complexes to Cpx. Surprisingly, the addition of Cpx caused the unzipping to occur at higher force levels (Fig. 1c, e, blue arrows). This Cpx-dependent resistance of the SNARE complex to high forces was consistently observed across different force-loading frequencies (Supplementary Fig. 4). Furthermore, when we examined the force - extension curves closely, we discovered that Cpx suppresses the reversible transitions significantly before unzipping (Fig. 1e versus 1d, red circles), meaning that Cpx affects the conformation of the tweezed SNARE complexes prior to unzipping. We gathered the force levels at which the unzipping events occurred from repeated stretching and relaxation periods (Fig. 1f). The unzipping force differed randomly between trials, suggesting stochastic energy barrier crossings.

When the unzipping force distributions were compared, it was discovered that in the presence of Cpx, the unzipping occurred

at 2 pN higher force levels on average (Fig. 1f). Surprisingly, the existence of Cpx resulted in a wider distribution of unzipping force, implying more heterogeneous rupture events at the single-molecule stage. The rezipping power, on the other hand, did not alter significantly after Cpx was added (Supplementary Fig. 4). Overall, our findings indicate that Cpx improves the mechanical stability of the neuronal SNARE complex.

3. Cpx extends the lifetimes of zippered SNAREs under tension.

We used force-jump experiments to test the lifetimes of zippered and unzipped SNARE complexes under stress to quantify the stabilization of SNARE complexes by Cpx (Fig. 2). With simple instrumentation, the magnetic tweezers allowed for quick adjustments and stable maintenance of force levels. We tested the latency to unzipping, then increased the load on a fully assembled SNARE complex from 10 to 14 pN rapidly within 100 ms (Fig. 2a). To test the latency in rezipping, τ rezip, we reversed the force scheme and suddenly reduced the force from 14 to 10 pN.

At 14 pN, the SNARE complexes unzipped mostly in a few seconds without Cpx (Fig. 2a). The addition of 5μM Cpx, on the other hand, greatly increased the time it took to τunzip to hundreds of seconds (Fig. 2b). The unzipping continued in the presence of Cpx, but at forces greater than 14 pN, and adding 15 pN shortened the unzip to a timescale that could be

measured experimentally (Fig. 2c). All of the τunzip distributions obtained at various force levels followed single-exponential distributions (Fig. 2d), implying that there is only one significant energy barrier to unzipping. The logarithms of the unzipping rates is linearly related to the applied force (Fig. 2e), confirming the Bell equation's validity even in the presence of Cpx[43,44] molecular behavior (Supplementary Note 4). Cpx delayed the unzipping of SNARE complexes by nearly two orders of magnitude across the force spectrum we investigated, according to a comparison of unzipping speeds (Fig. 2e).

The observed τrezip values also followed single exponential distributions, yielding SNARE zippering rates at varying forces (Fig. 2f). The logarithms of the rezipping rates decreased linearly with the applied force again as predicted by the Bell equation (Fig. 2g). However, the presence of Cpx did not appreciably change τrezip, consistent with the invariance of rezipping force distribution (Supplementary Fig. 4).

We calculated the distances and heights of the energy barriers crossed during the unzipping and rezipping of a single neuronal SNARE complex using the linear dependences of the logarithms of the kinetic rates on the applied mechanical tension (Fig. 2e, g). In the presence or absence of Cpx, we show a coarse-grained sketch of this energy landscape (Fig. 2h; we used a pre-exponential factor of 10^6 s^{-1} as is commonly accepted[33,34]). The zippered condition in this energy landscape applies to all conformations prior to the main unzipping, including fully assembled and partially unzipped forms (see Fig.

3 below). The zippered state becomes less stable and energetically equivalent to the unzipped state as more force is applied (Fig. 2h). The energy barrier to unzipping was calculated to be 15 k_BT high. Importantly, Cpx increased the barrier for unzipping to 19 k_BT by stabilizing the zippered state by 4.3 0.5 k_BT (error: 95 percent CI). This accounts for the longer lifetimes of zippered SNARE complexes (Fig. 2h, blue versus black curves). The existence of Cpx, on the other hand, had no effect on the unzipped state. Our findings indicate that Cpx has a significant impact on the energy landscape regulating the assembly and disassembly of the neuronal SNARE complex.

4. Cpx affects unzipping intermediates of a SNARE complex.

So far, we've just looked at Cpx's mechanical stabilization of SNARE complexes. However, there were two observations that this stabilizing effect could not account for. Cpx first moved the coarse-grained zippered state of the SNARE complex by around 2 nm away from the unzipped state (Fig. 2h). Second, we discovered that Cpx suppresses the fluctuations in the SNARE complex prior to the key unzipping event in the force-ramp experiments shown in Fig. 1. These findings may indicate that Cpx has an effect on the formation of SNAREs before they are unzipped[40].

As a result, we used a higher sampling rate of 1.2 kHz to overcome the intermediate conformations of single SNARE complexes (Fig. 3a). To induce SNARE complex unzipping, we

repeated our force-jump experiments in Fig. 2a, raising the stress from 10 to 14 pN. The extension values of a single SNARE complex sampled at 14 pN generated a mixture of Gaussian distributions in the absence of Cpx (Fig. 3a). The value of the high sampling rate is highlighted by the fact that these components were not resolved by our previous 100-Hz monitoring of the beads (Supplementary Fig. 5).

The completely zippered SNARE complex had the lowest peak, which we described as 0 nm for simplicity. The next two peaks, at 5.3 and 13.0 nm, corresponded to the predicted lengths for the linker-open (5.4 nm) and half-zippered (13.0 nm) states, respectively (Fig. 3b versus 3a; see Supplementary Note 3 for calculations of the expected lengths). We assumed completely folded four-helix bundles of SNARE motifs and random-coil linker domains void of secondary structures for the linker-open conformation (Fig. 3b)[34,45]. Unzipping of synaptobrevin-2 and Q-SNARE proteins up to the +2 and +4 layers, respectively, was included in the half-zippered state11,37,46. After the key unzipping, the peak was measured at 28.5 nm. Total unraveling of synaptobrevin-2 and further unfolding of the Q-SNARE proteins to the zeroth layer, which was calculated to be at 26.7 nm, better matched this extension (Fig. 3b versus 3a and Supplementary Fig. 3).

Surprisingly, the extension distribution observed under 14 pN changed dramatically when 5μM Cpx was applied. The linker-open state's population grew at the detriment of the completely zippered and half-zippered states (Fig. 3c versus 3a).

We repeated the experiment at a higher force level of 14.8 pN to see if this result was a unique feature at 14 pN. The linker-open population grew even more, while the other conformations were only adopted for a short time, reaffirming Cpx's promotion of the linker-open state (Fig. 3d).

We examined the inter-mediate populations while gradually increasing the applied tension to systematically evaluate this pattern (Fig. 3e, f, and Supplementary Note 5). To cause any partial unzipping of the SNARE complex in the absence of Cpx, at least 13 pN was necessary. Both the linker-open and half-zippered states populated with increasing stress above 13 pN. (Fig. 3e, upper panels). The unzipped intermediates were visible again in the presence of Cpx at 13 pN, indicating the same threshold force level as before Cpx (Fig. 3e, f). At forces above 14.5 pN, however, the linker-open population was significantly promoted, while the half-zippered state was largely unchanged, leaving the linker-open conformation as the only abundant species (Fig. 3e, lower panels). Cpx had little impact on the distance between the completely zippered and linker-open states (Supplementary Fig. 6), meaning that the linker-open conformation was mostly conserved.

5. Linker-open state is promoted in unzipping and zippering.

We wondered if the same results would be repeated during a zippering process because the promotion of linker-open state by Cpx was observed during unzipping processes. We first induced

complete unzipping of a SNARE complex at 16 pN, then lowered the tension to 14 pN and waited for a rezipping case (Fig. 3g). The zippering reaction was not only slow above 13 pN, but it was also slowed by SNAP-25 dissociation, particularly without Cpx. Nonetheless, at or above 14 pN, we were able to detect certain zippering cases. The SNARE complex rezipped after a long latency and showed transitions between intermediates when it was successful (Fig. 3g). It's worth noting that the rezipped SNARE complex's extension distribution was nearly identical to that seen during the unzipping phase (Fig. 3g versus 3a, and Fig. 3h).

Then, for SNARE rezipping, we added 5μM Cpx to this force-jump scheme (Fig. 3i). Importantly, we discovered that Cpx's effects appeared immediately after rezipping within our time resolution (830μs), displaying an enhanced linker-open population while suppressing the half-zippered state. We also confirmed that at 14.8 pN of tension, the linker-open state was the only prevailing conformation (Fig. 3j). The promotion of the linker-open state through the suppression of the other states was essentially replicated in this rezipping experiment. Indeed, the conformational distributions observed during the unzipping and rezipping experiments were very similar (Fig. 3h), implying that the quick exchanges among the intermediates take place close to equilibrium. In other words, regardless of how we applied the force, the relative populations were solely determined by the moment-to-moment stress.

When the two apparently contradictory effects of Cpx were

combined, they became clear. On the one side, Cpx virtually eliminated the half-zipped population across the entire force spectrum we investigated (Fig. 3f, orange), which is consistent with Cpx's stabilizing function in Figs. 1 and 2. Cpx, on the other hand, increased the linker-open population preferentially, preventing the SNARE complex assembly from being completed (Fig. 3f, magenta). The first effect aids the zippering of SNARE motifs, while the second effect causes the linker regions to be partially zippered. Cpx's two activities together resulted in the linker-open conformation of single neuronal SNARE complexes being clamped.

6. Kinetics of Cpx-mediated linker-open SNARE complex

We used hidden Markov modeling (HMM) on high-speed traces recorded with or without Cpx to better understand the kinetics of exchanges among conformational intermediates (Fig. 4a and Supplementary Note 6). We used a few parameters from the calculated extension distributions for the three conformational intermediates (Fig. 3e) as prior inputs in the HMM analysis, such as the means and variances of the Gaussian distributions representing respective intermediates. All transitions between intermediates were defined using the HMM technique, and the corresponding kinetic rates were calculated (Fig. 4a). All of the obtained kinetic rates were in the range of 1 to 10^3 s^{-1}, as calculated reliably by our 1.2-kHz time traces (Fig. 4b - e).

The zippering rate of the C-terminal half of SNARE motifs

(i.e., the transition rate from the half-zipped to the linker-open state) was increased by Cpx, according to the HMM study (Fig. 4b). Cpx, on the other hand, significantly decreased the unzipping rate for the C-terminal portion (Fig. 4c). As a result, Cpx not only facilitated the zippering of the C-terminal half of SNARE motifs, but it also prevented the unzipping of the same region, resulting in the observed stabilization.

Cpx slowed the zippering of linker domains (the transition from the linker-open to the completely zippered state) in line with the observed promotion of the linker-open state (Fig. 4d). Cpx, on the other hand, had only a minor effect on the unzipping rate of the linker domains (Fig. 4e), implying a very passive role for Cpx in the inhibition of linker domain assembly. We observed that in the high-force regime we investigated, the loaded tension's unzipping impact would outweigh any destabilizing effect of Cpx. On the contrary, extrapolation of Fig. 4e towards 0 pN suggests that the unzipping would become substantially faster in the presence of Cpx albeit on much longer time scales (Supplementary Fig. 7a), implying that Cpx might actively open the linker domains in such a low-force regime. This finding is in line with a previous single-molecule fluorescence resonance energy transfer (FRET) analysis, which found that Cpx[40] reduces FRET efficiency at the C-terminal ends of SNAREs. Together, these kinetic analyses revealed the details of how Cpx enables the focused clamping of neuronal SNARE complexes in the linker-open state (Supplementary Fig. 7 and Supplementary Table 2).

7. Differential regulation of SNARE complex by domains of Cpx

To figure out the domains of Cpx are responsible for its dual functionality, we created truncated Cpx variants that are missing domains sequentially from their ends (Fig. 5a and Supplementary Fig. 1). As shown in Fig. 1, we first looked at these variants in force ramps and compared their force–extension curves (Fig. 5b). All of the Cpx models, including the central helix-only build (dubbed "C"), showed an improvement in unzipping force. This means that the central helix's attachment to the SNARE complex[19,20] is critical for stabilization.

The force-dependent equilibrium of the zippered intermediates for the same Cpx variants was then investigated. To demarcate the evolution of intermediate populations with increasing power, we fitted the distributions of their extension values to three Gaussian distributions (Fig. 5c–f; see Supplementary Fig. 7 and Supplementary Table 2 for related HMM analyses). The suppression of the half-zippered state was found to be primarily dependent on Cpx's central helix. At 14 pN, the solitary central helix, for example, significantly decreased the half-zippered population (Fig. 5e; C versus None). Furthermore, the accessory helix was needed to extinguish the remaining half-zippered population (Fig. 5e; AC versus C), implying that the central and accessory helices collaborate to stabilize the four-helix bundle of SNARE motifs. With the sequential addition of the central

and accessory helices, we found a combined suppression of the half-zippered condition while analyzing individual traces (Fig. 5g). The linker-open population, in which wild-type (WT) Cpx clamped the SNARE complex, was then investigated (Fig. 5d, f). The existence of the N-terminal domain, in particular, more than tripled the linker-open population at 14 pN, suggesting that Cpx's ability to interfere with linker domains was heavily reliant on its N-terminal domain (Fig. 5f; WT/NAC versus AC). In fact, the linker-open populations for the AC and C variants were smaller than those generated without Cpx (Fig. 5f). This effect could be seen also at the level of individual high-speed traces (Fig. 5h), demonstrating that Cpx's stabilizing operation takes precedence when the N-terminal domain is absent.

Finally, deletion of the C-terminal domain had no impact on any of the aspects of Cpx feature we looked at (Fig. 5b - h; WT versus NAC), which is consistent with the domain's recorded independent position in membrane binding and fusion site localization[47,48].

Discussion

The assembly of neuronal SNARE complexes catalyzes synaptic vesicle fusion, one of the quickest exocytosis processes observed in biological systems. Cpx is the only presynaptic protein known to bind strongly to the SNARE complex, increasing the likelihood that Cpx modulates SNARE assembly directly. We discovered that Cpx significantly improves the

mechanical stability of single SNARE complexes using magnetic tweezers. Cpx physically protects the four-helix bundle of SNARE motifs[20], which is consistent with previous deuterium exchange results. Furthermore, we discovered that Cpx plays an unexpected role in actively driving SNARE complexes into linker-open conformation. Despite the fact that our findings are focused on rat Cpx and SNARE proteins, the results are likely to be similar in human proteins since only five amino acid residues differ (see Methods). Despite the fact that the linker domains of SNAREs form a coiled-coil structure that extends the helical structure of the SNARE complex up to the transmembrane domains[49], their significance has been overlooked in comparison to the SNARE motifs. We propose that the linker domains can represent the final molecular switch of the neuronal SNARE complex that must be zippered to achieve complete synaptic vesicle fusion[22,34,49,50], based on our observation that Cpx serves as a centered clamp for the SNARE complexes in linker-open conformation (Fig. 6, left). Indeed, a mutation in the linker region of synaptobrevin-2 causes the loss-of-function phenotype of Cpx in murine hippocampal neurons, implying that Cpx regulates force transfer from SNARE motifs to fusing membranes[22]. We discovered that above 14 pN, the linker-open state becomes most populated, and that this state will divide the two fusing membranes by about 6 nm. This physical distance, which is similar to what has been observed in electron microscopy studies[51,52], may act as a crucial barrier, preventing spontaneous fusion beyond what

is functionally needed.

We discovered that mechanical tension had only a limited impact on single SNARE complexes, namely between 13 and 16 pN. When the stress was less than 13 pN, there was no discernible conformational change in the fully assembled SNAREs. The SNARE complex started sampling intermediate conformations, such as the linker-open and half-zippered states, at only 13 pN. Even in the presence of Cpx, synaptobrevin-2 easily unraveled from the Q-SNAREs beyond 16 pN, and all SNAREs unfolded in turn. This finding suggests that tensions greater than 16 pN are either not reached during synaptic vesicle fusion, are unrelated to the activity of the neuronal SNARE complex, or both. As a result, the force range of 13 to 16 pN most likely corresponds to the most critical regime in which individual SNARE complexes dynamically sample multiple conformations.

Surprisingly, all of the molecular effects of Cpx that we saw occurred within this small range of strain. Cpx's work was thus devoted to altering the balance of SNARE complexes' con- formational intermediates. The molecular behavior of Cpx's different domains were discovered to work together to promote the linker-open conformation, which is the only abundant state above 14 pN stress. Cpx is inherently equipped to work with neuronal SNARE complexes under a well-defined spectrum of mechanical stress, according to these findings.

What are the implications of these findings in a force-loaded setting for synaptic vesicle fusion in the physiological

environment? Transitions between conformational intermediates took place near equilibrium, making the relative populations of intermediates independent of force background. The similarity of intermediate populations in unzipping and rezipping experiments confirmed this hypothesis. As a result, if a single neuronal SNARE complex experiences tensions above 13 pN at synapses is a significant physical condition that validates the physiological validity of our observation. Although the repulsive force between a synaptic vesicle and a presynaptic membrane has yet to be measured experimentally, it is expected to rapidly build up upon close apposition of the two charged membranes[31], reaching 13 pN at a separation of 2 - 3 nm (Supplementary Fig. 8). As a result, we believe that the effects of Cpx mentioned here will manifest as soon as the linker domains of SNAREs attempt to zipper, providing a point for timely and efficient membrane fusion regulation. In this regard, it's noteworthy that we were able to confirm Cpx's effects during the zippering of SNARE complexes, which resembles the initial docking of synaptic vesicles to the membrane in neurons.

Surprisingly, we discovered that Cpx's dual function was due to different domains within the protein. The central and accessory helices of Cpx, which buttressed the four-helix bundle of SNARE motifs, were primarily responsible for the stabilizing effect. The N-terminal domain, on the other hand, suddenly mediated the clamping mechanism by interfering with the zippering of SNARE linker domains. Given that the N-terminal region of Cpx is thought to play a stimulatory role

in activated neurotransmission[17,23,24], this finding is quite unexpected.

We should point out that our experiments were conducted without the use of phospholipid membranes, obviating the possibility of observing any membrane-related effects. We propose that the clamping and stimulatory functions of the N-terminal domain manifest in a sequential manner along the steps of synaptic vesicle fusion, rather than interfering with one another. The N-terminal domain of Cpx would be 3 nm away from the fusing membranes in the primed, linker-open state, and preferentially interact with the linker domains of SNAREs. SNAREs will zipper even more during fusion, allowing contact between membrane and Cpx and liberating Cpx's53 stimulatory impact.

A Ca2+ influx could cause the final phase of fusion in two ways, according to our speculation (Fig. 6, right). Ca2+-responsive factors like synaptotagmin[54 - 60] can dislodge the N-terminus of Cpx from a SNARE complex in one scenario. This release allows SNAREs' linker domains to fully zipper, effectively driving full zippering of SNAREs even without lowering stress. In a different example, the Ca2+ sensor could act as a bridge between the two fusing mem- branes61 - 65, effectively lowering the tension applied to each SNARE complex. Regardless of Cpx, if this stress is reduced below 13 pN, the SNARE complex will strongly favor the completely zippered state. Without any interaction between Cpx and the Ca2+-responsive factors, full synaptic vesicle fusion will occur.

Finally, our findings support the hypothesis that the synaptic fusion machinery is a complex mechanical mechanism built to achieve membrane fusion in a millisecond while simultaneously clamping unwanted vesicle release. Our findings indicate that in the presence of physiologically significant levels of mechanical stress, the interactions of neuronal SNARE complexes with their regulators must be understood. Just a few piconewtons of mechanical stress, induced by fusion regulators, is needed to unlock the zippering potential of neuronal SNAREs and drive synchronous neurotransmitter release. Furthermore, these results also can be applied to design protein drugs that inhibit or stimulate SNARE complex formation by engineering complexin.

참 고 문 헌

References 1. Südhof, T. C. The synaptic vesicle cycle: a cascade of protein-protein interactions. Nature 375, 645 - 653 (1995).

2. Weber, T. et al. SNAREpins: minimal machinery for membrane fusion. Cell 92, 759 - 772 (1998).

3. Jahn, R. & Fasshauer, D. Molecular machines governing exocytosis of synaptic vesicles. Nature 490, 201 - 207 (2012).

4. McMahon, H. T., Missler, M., Li, C. & Südhof, T. C. Complexins: cytosolic proteins that regulate SNAP receptor function. Cell 83, 111 - 119 (1995).

5. Trimbuch, T. & Rosenmund, C. Should I stop or should I go? The role of complexin in neurotransmitter release. Nat. Rev. Neurosci. 17, 118 - 125 (2016).

6. Brunger, A. T., Leitz, J., Zhou, Q., Choi, U. B. & Lai, Y. Ca2+-triggered synaptic vesicle fusion initiated by release of inhibition. Trends Cell Biol. 28, 631 - 645 (2018).

7. Schneggenburger, R. & Rosenmund, C. Molecular mechanisms governing Ca (2+) regulation of evoked and spontaneous release. Nat. Neurosci. 18, 935 - 941 (2015).

8. Reim, K. et al. Complexins regulate a late step in Ca2+-dependent neurotransmitter release. Cell 104,71 - 81 (2001).

9. Giraudo, C. G., Eng, W. S., Melia, T. J. & Rothman, J. E. A clamping mechanism involved in SNARE-dependent exocytosis. Science 313, 676 - 680 (2006).

10. Huntwork, S. & Littleton, J. T. A complexin fusion clamp regulates spontaneous neurotransmitter release and synaptic growth. Nat. Neurosci. 10, 1235 - 1237 (2007).
11. Trimbuch, T. et al. Re-examining how complexin inhibits neurotransmitter release. eLife 3, e02391 (2014).
12. Xue, M. et al. Tilting the balance between facilitatory and inhibitory functions of mammalian and Drosophila complexins orchestrates synaptic vesicle exocytosis. Neuron 64, 367 - 380 (2009).
13. Cho, R. W., Song, Y. & Littleton, J. T. Comparative analysis ofDrosophila and mammalian complexins as fusion clamps and facilitators of neurotransmitter release. Mol. Cell. Neurosci. 45, 389 - 397 (2010).
14. Radoff, D. T. et al. The accessory helix of complexin functions by stabilizing central helix secondary structure. eLife 3, e04553 (2014).
15. Krishnakumar, S. S. et al. Re-visiting the trans insertion model for complexin clamping. eLife 4, e04463 (2015).
16. An, S. J., Grabner, C. P. & Zenisek, D. Real-time visualization of complexin during single exocytic events. Nat. Neurosci. 13, 577 - 583 (2010).
17. Xue, M. et al. Distinct domains of complexin I differentially regulate neurotransmitter release. Nat. Struct. Mol. Biol. 14, 949 - 958 (2007).
18. Lai, Y. et al. Complexin inhibits spontaneous release and synchronizes Ca2 +-triggered synaptic vesicle fusion by distinct mechanisms. eLife 3, e03756 (2014).
19. Pabst, S. et al. Selective interaction of complexin with the neuronal SNARE complex. Determination of the binding

regions. J. Biol. Chem. 275, 19808 - 19818 (2000).
20. Chen, X. et al. Three-dimensional structure of the complexin/SNARE complex. Neuron 33, 397 - 409 (2002).
21. Zhou, Q. et al. The primed SNARE-complexin-synaptotagmin complex for neuronal exocytosis. Nature 548, 420 - 425 (2017).
22. Maximov, A., Tang, J., Yang, X., Pang, Z. P. & Südhof, T. C. Complexin controls the force transfer from SNARE complexes to membranes in fusion. Science 323, 516 - 521 (2009).
23. Lai, Y. et al. N-terminal domain of complexin independently activates calcium-triggered fusion. Proc. Natl Acad. Sci. USA 113, E4698 - E4707 (2016).
24. Xue, M. et al. Binding of the complexin N terminus to the SNARE complex potentiates synaptic-vesicle fusogenicity. Nat. Struct. Mol. Biol. 17, 568 - 575 (2010).
25. Giraudo, C. G. et al. Alternative zippering as an on-off switch for SNARE- mediated fusion. Science 323, 512 - 516 (2009).
26. Yang, X., Kaeser-Woo, Y. J., Pang, Z. P., Xu, W. & Südhof, T. C. Complexin clamps asynchronous release by blocking a secondary Ca(2+) sensor via its accessory α helix. Neuron 68, 907 - 920 (2010).
27. Kümmel, D. et al. Complexin cross-links prefusion SNAREs into a zigzag array. Nat. Struct. Mol. Biol. 18, 927 - 933 (2011).
28. Li, F. et al. Complexin activates and clamps SNAREpins by a common mechanism involving an intermediate energetic state. Nat. Struct. Mol. Biol. 18, 941 - 946 (2011).
29. Snead, D., Wragg, R. T., Dittman, J. S. & Eliezer, D. Membrane curvature sensing by the C-terminal domain of complexin. Nat. Commun. 5, 4955 (2014).
30. Gong, J. et al. C-terminal domain of mammalian complexin-1

localizes to highly curved membranes. Proc. Natl Acad. Sci. USA 113, E7590 – E7599 (2016).

31. Bykhovskaia, M., Jagota, A., Gonzalez, A., Vasin, A. & Littleton, J. T. Interaction of the complexin accessory helix with the C-terminus of the SNARE complex: molecular-dynamics model of the fusion clamp. Biophys. J. 105, 679 – 690 (2013).
32. Oelkers, M., Witt, H., Halder, P., Jahn, R. & Janshoff, A. SNARE-mediated membrane fusion trajectories derived from force-clamp experiments. Proc. Natl Acad. Sci. USA 113, 13051 – 13056 (2016).
33. Min, D. et al. Mechanical unzipping and rezipping of a single SNARE complex reveals hysteresis as a force-generating mechanism. Nat. Commun. 4, 1705 (2013).
34. Gao, Y. et al. Single reconstituted neuronal SNARE complexes zipper in three distinct stages. Science 337, 1340 – 1343 (2012).
35. Ryu, J.-K. et al. Spring-loaded unraveling of a single SNARE complex by NSF in one round of ATP turnover. Science 347, 1485 – 1489 (2015).
36. Sørensen, J. B. et al. Sequential N- to C-terminal SNARE complex assembly drives priming and fusion of secretory vesicles. EMBO J. 25, 955 – 966 (2006).
37. Ma, L. et al. Munc18-1-regulated stage-wise SNARE assembly underlying synaptic exocytosis. eLife 4, e09580 (2015).
38. Zorman, S. et al. Common intermediates and kinetics, but different energetics, in the assembly of SNARE proteins. eLife 3, e03348 (2014).
39. Li, F. et al. Energetics and dynamics of SNAREpin folding across lipid bilayers. Nat. Struct. Mol. Biol. 14, 890 – 896 (2007).
40. Choi, U. B., Zhao, M., Zhang, Y., Lai, Y. & Brunger, A. T.

Complexin induces a conformational change at the membrane-proximal C-terminal end of the SNARE complex. eLife 5, e16886 (2016).

41. Pabst, S. et al. Rapid and selective binding to the synaptic SNARE complex suggests a modulatory role of complexins in neuroexocytosis. J. Biol. Chem. 277, 7838 – 7848 (2002).
42. Li, Y., Augustine, G. J. & Weninger, K. Kinetics of complexin binding to the SNARE complex: correcting single molecule FRET measurements for hidden events. Biophys. J. 93, 2178 – 2187 (2007).
43. Bell, G. I. Models for the specific adhesion of cells to cells. Science 200, 618 – 627 (1978).
44. Tinoco, I. & Bustamante, C. The effect of force on thermodynamics and kinetics of single molecule reactions. Biophys. Chem. 101 – 102, 513 – 533 (2002).
45. Choi, U. B., McCann, J. J., Weninger, K. R. & Bowen, M. E. Beyond the random coil: stochastic conformational switching in intrinsically disordered proteins. Structure 19, 566 – 576 (2011).
46. Zhang, X. et al. Stability, folding dynamics, and long-range conformational transition of the synaptic t-SNARE complex. Proc. Natl Acad. Sci. USA 113, E8031 – E8040 (2016).
47. Wragg, R. T. et al. Synaptic vesicles position complexin to block spontaneous fusion. Neuron 77, 323 – 334 (2013).
48. Diao, J. et al. Complexin-1 enhances the on-rate of vesicle docking via simultaneous SNARE and membrane interactions. J. Am. Chem. Soc. 135, 15274 – 15277 (2013).
49. Stein, A., Weber, G., Wahl, M. C. & Jahn, R. Helical extension of the neuronal SNARE complex into the membrane. Nature 460,

525 – 528 (2009).

50. Hernandez, J. M. et al. Membrane fusion intermediates via directional and full assembly of the SNARE complex. Science 336, 1581 – 1584 (2012).

51. Imig, C. et al. The morphological and molecular nature of synaptic vesicle priming at presynaptic active zones. Neuron 84, 416 – 431 (2014).

52. Gipson, P. et al. Morphologies of synaptic protein membrane fusion interfaces. Proc. Natl Acad. Sci. USA 114, 9110 – 9115 (2017).

53. Prinslow, E. A., Brautigam, C. A. & Rizo, J. Reconciling isothermal titration calorimetry analyses of interactions between complexin and truncated SNARE complexes. eLife 6, e30286 (2017).

54. Geppert, M. et al. Synaptotagmin I: a major Ca2+ sensor for transmitter release at a central synapse. Cell 79, 717 – 727 (1994).

55. Tucker, W. C., Weber, T. & Chapman, E. R. Reconstitution of Ca2+–regulated membrane fusion by synaptotagmin and SNAREs. Science 304, 435 – 438 (2004).

56. Bhalla, A., Chicka, M. C., Tucker, W. C. & Chapman, E. R. Ca(2+)–synaptotagmin directly regulates t–SNARE function during reconstituted membrane fusion. Nat. Struct. Mol. Biol. 13, 323 – 330 (2006).

57. Tang, J. et al. A complexin/synaptotagmin 1 switch controls fast synaptic vesicle exocytosis. Cell 126, 1175 – 1187 (2006).

58. Schaub, J. R., Lu, X., Doneske, B., Shin, Y.–K. & McNew, J. A. Hemifusion arrest by complexin is relieved by

Ca2+-synaptotagmin I. Nat. Struct. Mol. Biol. 13, 748 - 750 (2006).

59. Chicka, M. C., Hui, E., Liu, H. & Chapman, E. R. Synaptotagmin arrests the SNARE complex before triggering fast, efficient membrane fusion in response to Ca2+. Nat. Struct. Mol. Biol. 15, 827 - 835 (2008).

60. Zhou, Q. et al. Architecture of the synaptotagmin-SNARE machinery for neuronal exocytosis. Nature 525,62 - 67 (2015).

61. Araç, D. et al. Close membrane-membrane proximity induced by Ca(2 +)-dependent multivalent binding of synaptotagmin-1 to phospholipids. Nat. Struct. Mol. Biol. 13, 209 - 217 (2006).

62. Martens, S., Kozlov, M. M. & McMahon, H. T. How synaptotagmin promotes membrane fusion. Science 316, 1205 - 1208 (2007).

63. Hui, E., Johnson, C. P., Yao, J., Dunning, F. M. & Chapman, E. R. Synaptotagmin-mediated bending of the target membrane is a critical step in Ca(2+)-regulated fusion. Cell 138, 709 - 721 (2009).

64. van den Bogaart, G. et al. Synaptotagmin-1 may be a distance regulator acting upstream of SNARE nucleation. Nat. Struct. Mol. Biol. 18, 805 - 812 (2011).

65. Chang, S., Trimbuch, T. & Rosenmund, C. Synaptotagmin-1 drives synchronous Ca2+-triggered fusion by C2B-domain-mediated synaptic- vesicle-membrane attachment. Nat. Neurosci. 21,33 - 40 (2018).

66. Gosse, C. & Croquette, V. Magnetic tweezers: micromanipulation and force measurement at the molecular level. Biophys. J. 82, 3314 - 3329 (2002).

67. te Velthuis, A. J. W., Kerssemakers, J. W. J., Lipfert, J. &

Dekker, N. H. Quantitative guidelines for force calibration through spectral analysis of magnetic tweezers data. Biophys. J. 99, 1292 - 1302 (2010).

68. Daldrop, P., Brutzer, H., Huhle, A., Kauert, D. J. & Seidel, R. Extending the range for force calibration in magnetic tweezers. Biophys. J. 108, 2550 - 2561 (2015).

69. Chen, H. et al. Improved high-force magnetic tweezers for stretching and refolding of proteins and short DNA. Biophys. J. 100, 517 - 523 (2011).

70. Yang, W. Y. & Gruebele, M. Folding at the speed limit. Nature 423, 193 - 197 (2003).

Abstract

Mechanistic study on Complexin using magnetic tweezer

Haesoo Kim

Graduate School of Biological Sciences
Seoul National University

Through the development of SNARE complexes, neuronal soluble N-ethylmaleimide-sensitive factor attachment protein receptors (SNAREs) catalyze synaptic vesicle fusion with presynaptic membranes. The only presynaptic protein that tightly binds to SNAREs and regulates membrane fusion is Complexin (Cpx), but how it modulates the energy landscape of SNARE complex assembly, particularly under mechanical tensing, is unknown.

We show how Cpx interacts with single SNARE complexes using magnetic tweezers. Cpx's effects are only visible at high mechanical tensions above 13 pN. Cpx stabilizes the central four-helix bundle of SNARE motifs while also inhibiting linker-domain assembly, preventing complete zippering of SNAREs.

These findings indicate that in a linker-open conformation, Cpx generates a directed clamp for the neuronal SNARE complex. Our findings suggest that Cpx and neuronal SNAREs work together to prime synaptic vesicles in preparation for synchronous neurotransmitter release.

.....

keywords : Magnetic tweezer, Complexin, SNARE complex, neurotransmission, Force spectroscopy, neuroscience

student number : 2017-36517

Main figures

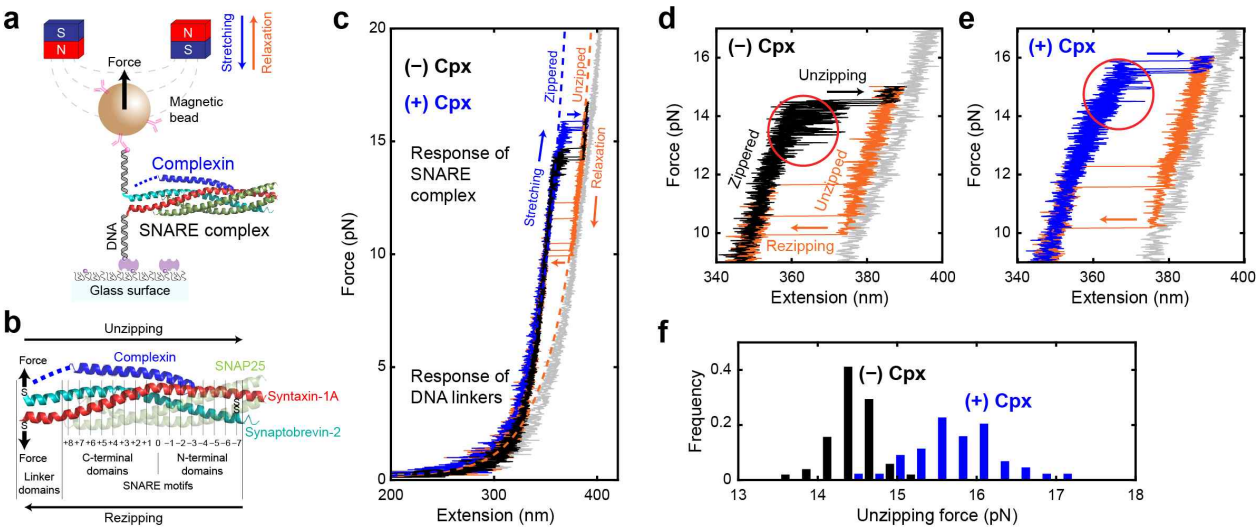

Fig. 1 Mechanical stabilization of SNARE complexes by complexin. a SNARE‐DNA hybrid construct in magnetic tweezers setup. b A predicted three‐ dimensional structure of the neuronal SNARE complex bound to a molecule of Cpx (PDB 3IPD49 aligned to 1KIL20). The N-terminal domain of Cpx not determined in the crystal structure (1‐25) is represented with a blue dashed line. The letters “S” denote the thiol groups of artificial cysteine residues. The numbers below the structure indicate the leucine-zipper layers. c Typical force‐extension curves from a single SNARE complex in the absence (black) and presence (blue) of Cpx. The black and blue traces show the stretching period that features “unzipping” events from the fully zippered to the unzipped state, while the orange traces show the relaxation period with the opposite “rezipping” events. In gray, a curve for the unfolded SNAREs that fail to re-zip is shown. Dashed lines indicate the models of extension for the corresponding conformations of SNARE complex (Supplementary Note 3). d, e Force‐extension curves from a single SNARE complex in the absence (d) or presence (e, same graph as in c) of Cpx. f Unzipping force distributions from a single SNARE complex in the absence (black, N= 51) and presence (blue, N= 44) of 5 μM Cpx

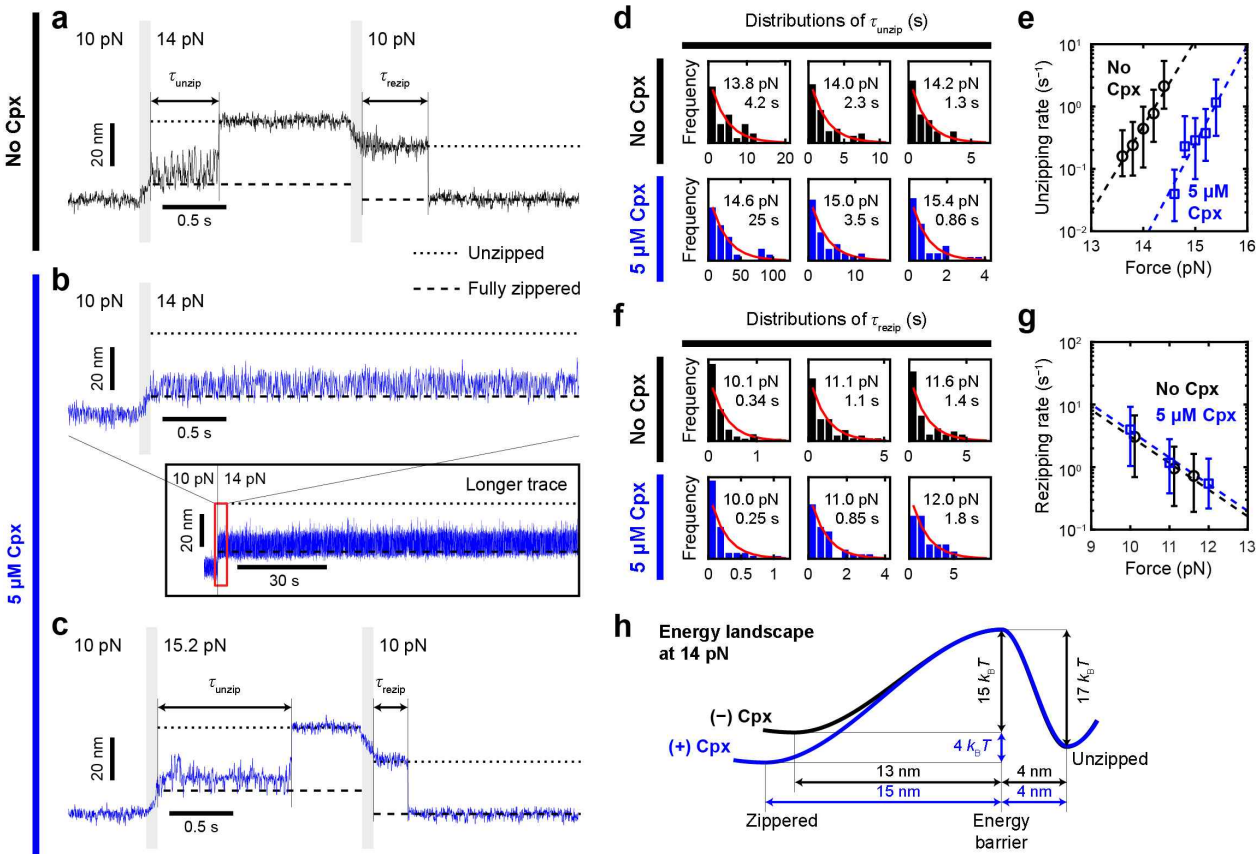

Fig. 2 Complexin extends the lifetime of zippered SNARE complexes under tension. a - c The force-jump scheme used for serial measurements of τunzip and τrezip in the absence (a) or presence (b, c) of Cpx. The predicted locations of the fully zippered and the unzipped states are indicated with dashed and dotted lines, respectively. Gray vertical bars mark the force-jump periods. Inset in b shows the marked increase in lifetime of SNARE induced by Cpx, the red box of which is magnified above. Vertical scale bars represent 20 nm, and horizontal scale bars represent 0.5 s (main panels) and 30 s (inset in b). d, f Distributions of τunzip (d) and τrezip (f) at varying forces (N≥ 19 for each panel). Red curves represent the fits to exponential distributions with their mean values indicated. e, g Force dependences of unzipping (e) and rezipping (g) rates in the absence (black) or presence (blue) of Cpx. Error bars represent the 95% confidence intervals for the mean parameter estimates in d and f. Dashed lines represent the fits to the Bell equation. h The energy diagram for the unzipping/zippering of a neuronal SNARE complex at 14 pN. The effect of Cpx is indicated in blue

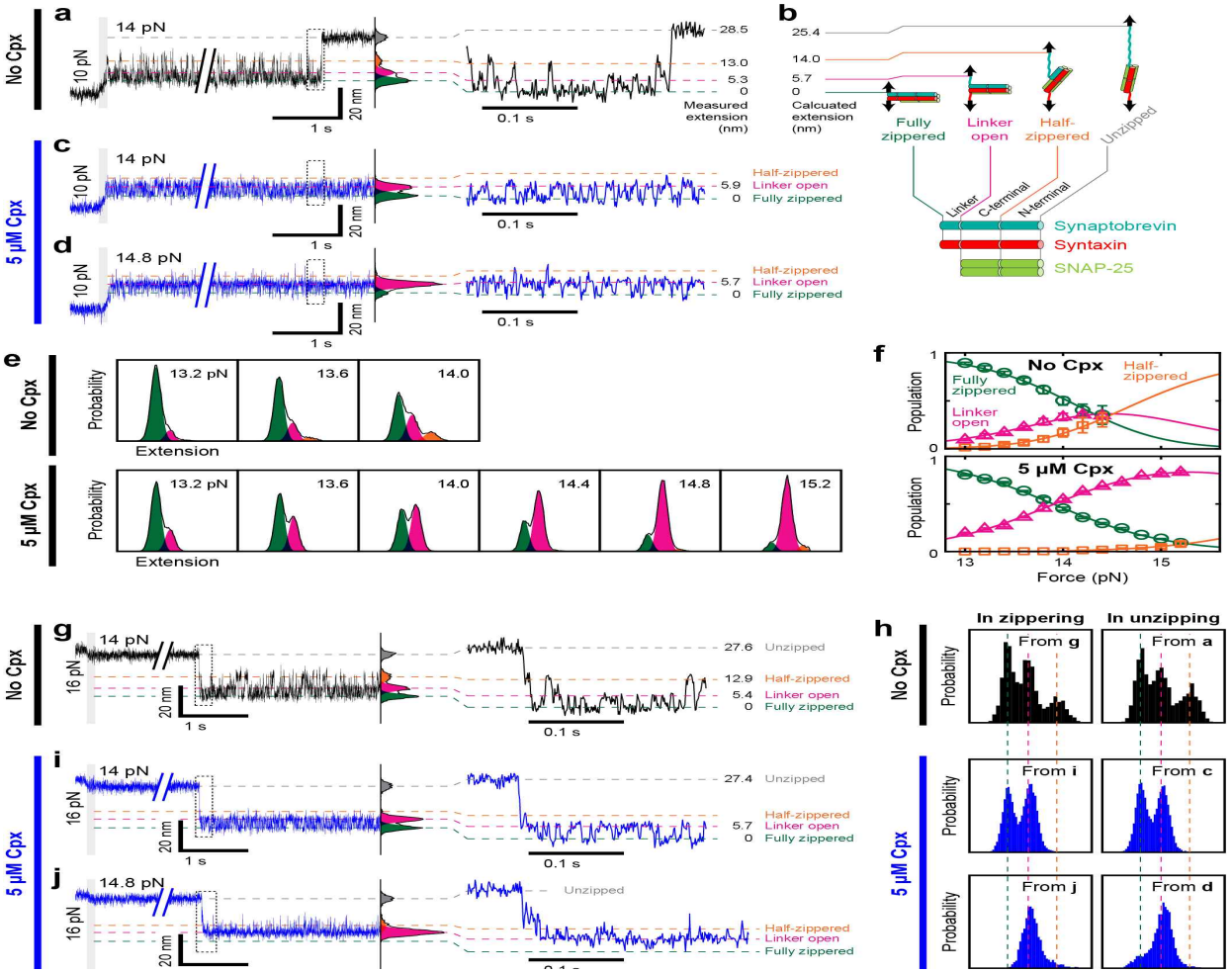

Fig. 3 Complexin promotes the linker-open state of neuronal SNARE complexes. a, c, d High-speed observations (1.2 kHz) of the conformational intermediates during the unzipping of a SNARE complex. The measured distributions of extensions (black lines displayed to the right of the traces) are overlaid with their identified Gaussian components color-coded green, magenta, orange, and gray from the lowest. Dotted areas are magnified on the right. The locations of the peaks are indicated with dashed lines of the same color and with numbers. b A model for the intermediate conformations of a SNARE complex with calculated values of extension. e Force-dependent shifts in extension distribution with the indicated Gaussian components. The color code is the same as in a–d. f Force-dependent equilibria among the three zippered conformations in the absence (upper) and presence (lower) of Cpx. Solid lines represent the fits to a three-state equilibrium model (Supplementary Note 5). Data are represented as mean ± s.d. of more than three measurements. g, i, j High-speed observations of the conformational intermediates during the zippering of a SNARE complex. The color code is the same as in a–f. h Comparisons of conformational equilibria during unzipping (upper; 10→14 pN) and zippering (lower; 16→14 pN) of a single SNARE complex. In all panels, vertical scale bars represent 20 nm. Horizontal scale bars represent 1 and 0.1 s (on left and right in a, c, d, g, i, j, respectively), and 10 nm (in e, h)

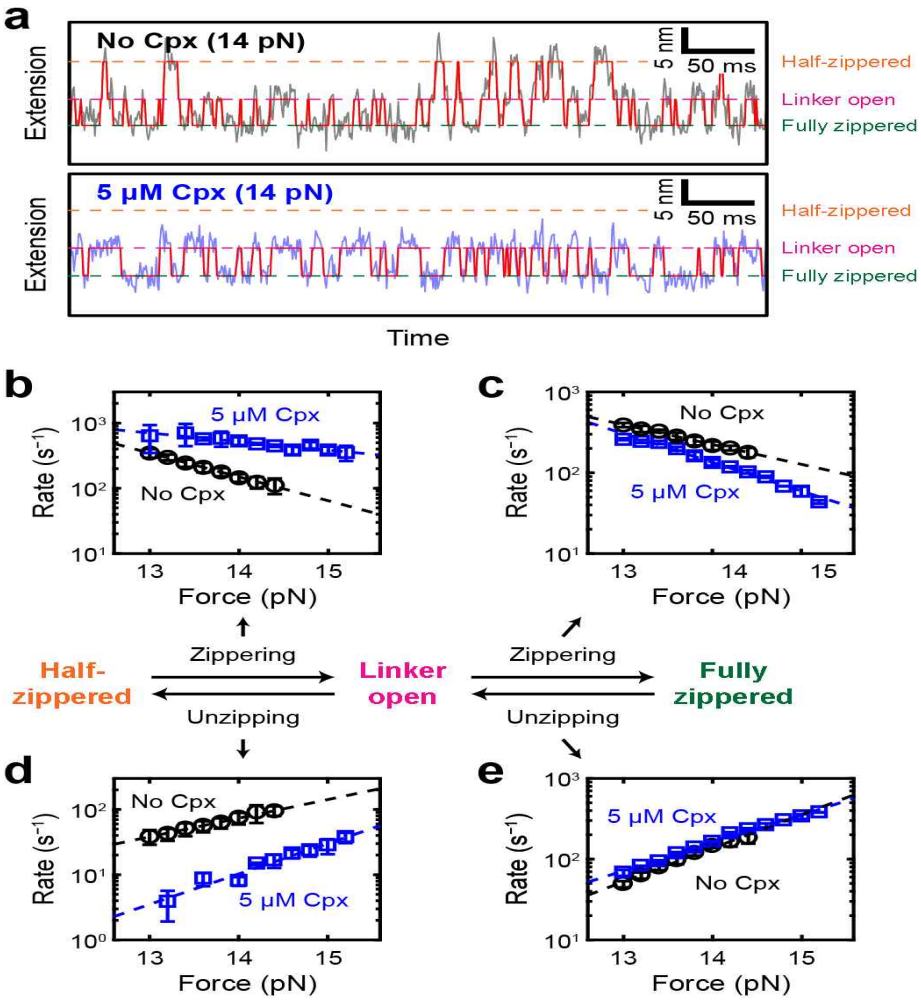

Fig. 4 Kinetic analysis of conformational intermediates through hidden Markov modeling. a Extension time traces measured at 1.2 kHz with a single SNARE complex in the absence (upper) or presence (lower) of 5 μM Cpx. The state paths obtained from hidden Markov modeling are overlaid in red (Supplementary Note 6). Vertical and horizontal scale bars represent 5 nm and 50 ms, respectively. b - e Force dependence of zippering (b, d) and unzipping (c, e) rates for C-terminal SNARE motifs (b, c) and linker domains (d, e) in the absence (black) or presence (blue) of 5 μM Cpx. Data are represented as mean ± s.d. of more than three measurements. Dashed lines represent the fits to the Bell equation. A diagram for the corresponding transitions in a SNARE complex is shown in the center

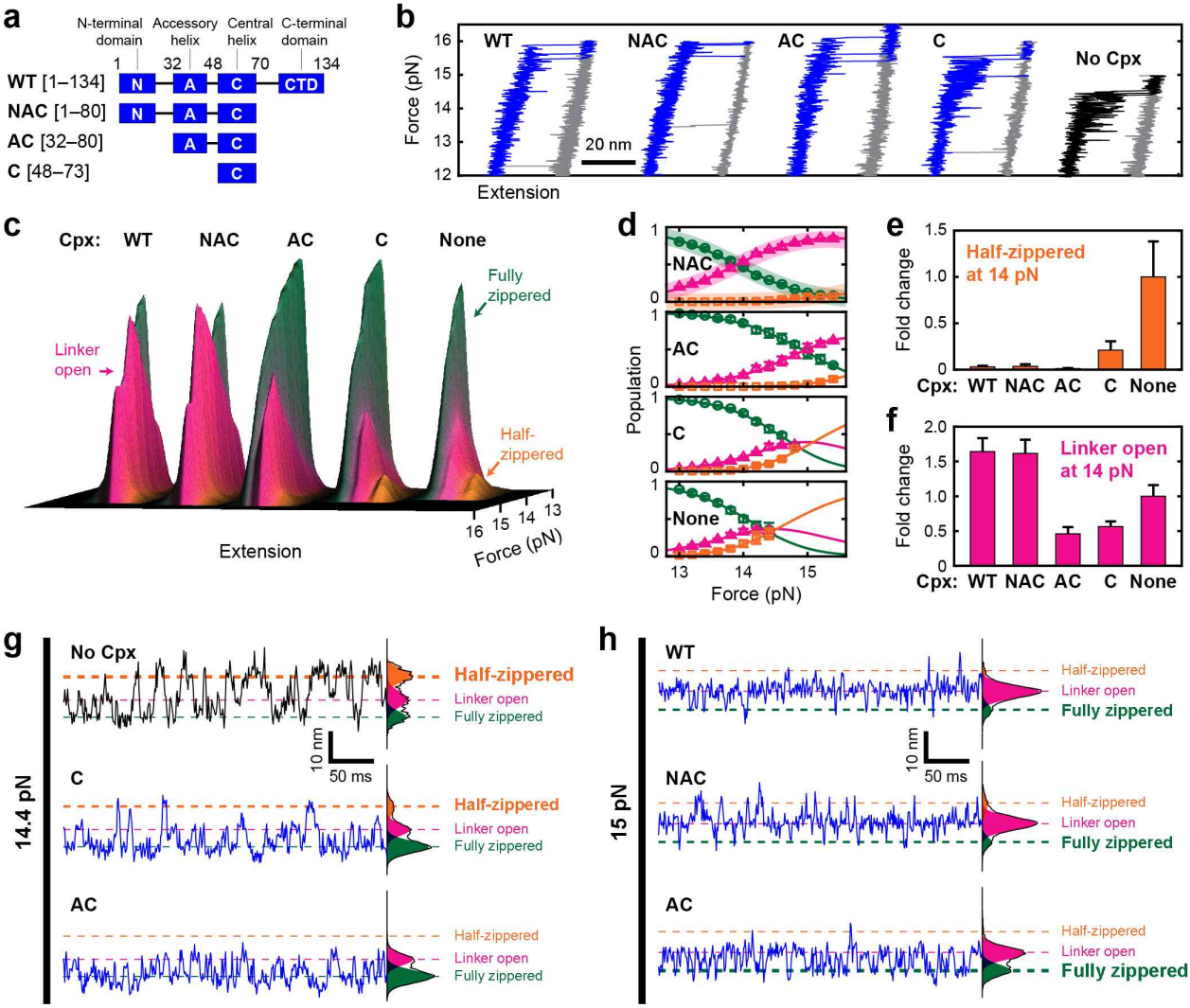

Fig. 5 Multiple domains of complexin collectively drives SNARE complexes into the linker-open conformation. a The domain structures of wild-type Cpx and its variants prepared in this study. b Force - extension curves for unzipping (blue/black) and rezipping (gray) of SNARE complexes in the presence of the indicated variants of Cpx (all at 5 μM). Horizontal scale bar represents 20 nm. c Force-dependent evolution of extensions for the SNARE complex between 13 and 16 pN of force in the presence of the indicated variants of Cpx. d Force-dependent equilibria among the three zippered conformations. Solid lines represent the fits to a three-state equilibrium model (Supplementary Note 5). The curves for wild-type Cpx (WT) are overlaid as shades in the top panel with NAC for the sake of comparison. The color code is the same as in c. e, f Fold changes at 14 pN in the half-zippered (e) and linker-open (f) populations upon addition of each Cpx variant. In d - f, data are represented as mean ± s.d. of more than three measurements. g, h Representative time traces for the SNARE complexes in the presence of the indicated variants of Cpx. Vertical and horizontal scale bars represent 10 nm and 50 ms, respectively.

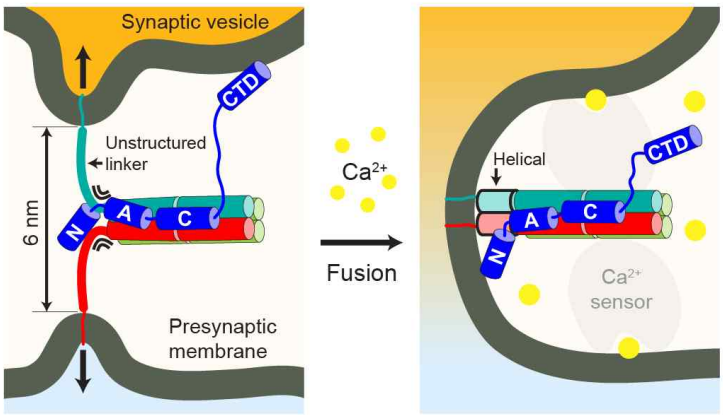

Fig. 6 A model for the function of complexin in synaptic vesicle fusion. (Left) A synaptic vesicle tethered to a presynaptic membrane via a Cpx - SNARE complex under a force-loaded environment. Cpx is shown in blue. (Right) Cpx - SNARE complex after a Ca2+-triggered membrane fusion event. A putative Ca2+ sensor in collaboration with the Cpx - SNARE complex is shown in gray.

SUPPLEMENTARY FIGURES

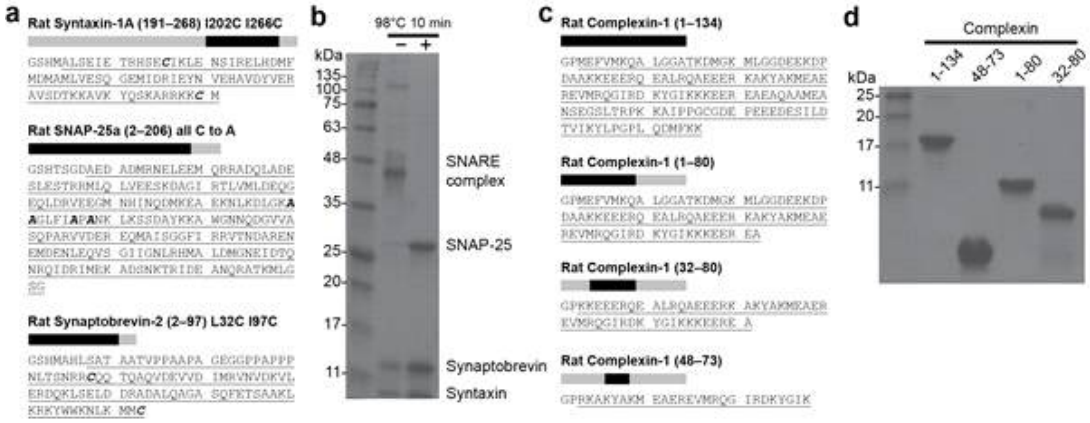

Supplementary Figure 1 Expression and purification of SNARE proteins and complexins. (a) Amino acid sequences of the SNARE proteins used in this study. (b) 12% SDS-PAGE gel images of either the assembled or the heat-disassembled SNARE complexes. (c) Amino acid sequences of the wild-type Cpx and truncation variants used in this study. (d) 20% SDS-PAGE gel for individual complexin variants. In (a) and (c), black bars mark the expressed region in the full-length wild-type sequence, and the underlined region belongs to the native sequence of the respective proteins.

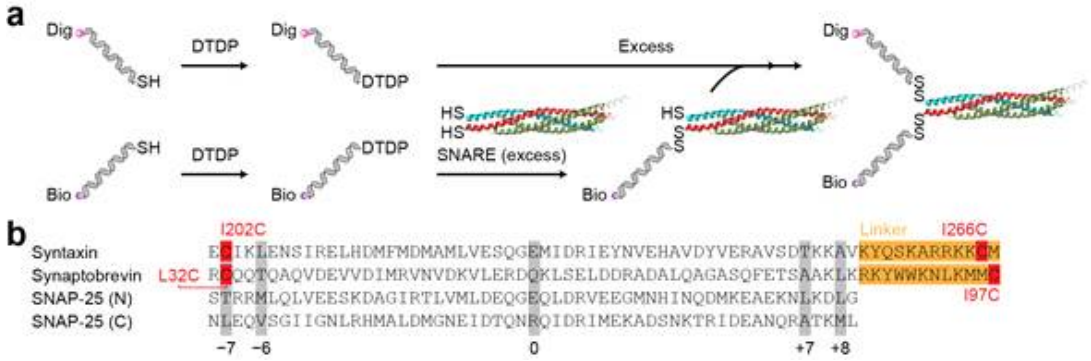

Supplementary Figure 2 Preparation of SNARE-DNA hybrid construct for magnetic tweezers experiments. (a) Scheme for the DNA handle attachment. The full details of the procedure are provided in Materials and Methods. (b) The location of residues for DNA handle attachment (I266 in syntaxin-1A and I97 in synaptobrevin-2) mutated to cysteine for disulfide linkage. Two additional residues in the N-termini of SNARE (I202 in syntaxin-1A and L32 in synaptobrevin-2) were mutated to cysteines and internally cross-linked via similar reaction for repeated measurements after unzipping of the SNARE complex.

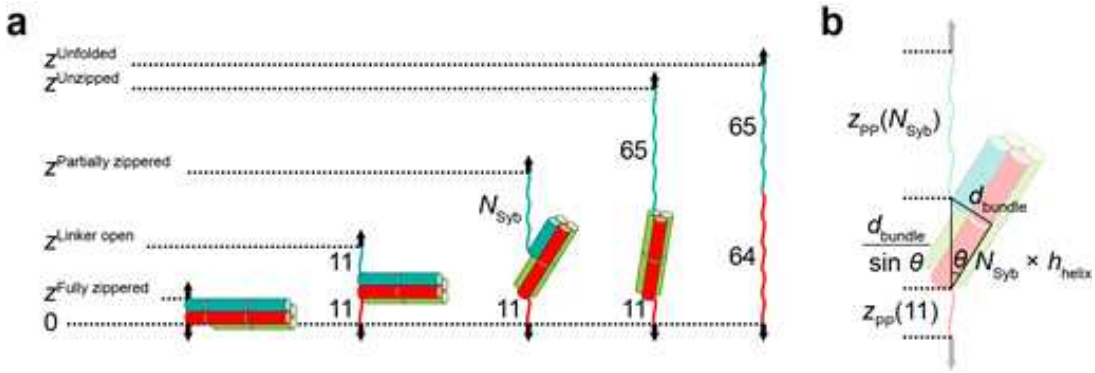

Supplementary Figure 3 Model of SNARE unzipping. (a) Intermediate conformations of a SNARE complex during unzipping. Numbers indicate the number of amino acids in the unfolded polypeptide segments at each conformation. (b) Detailed model for the extension in partially zippered conformation.

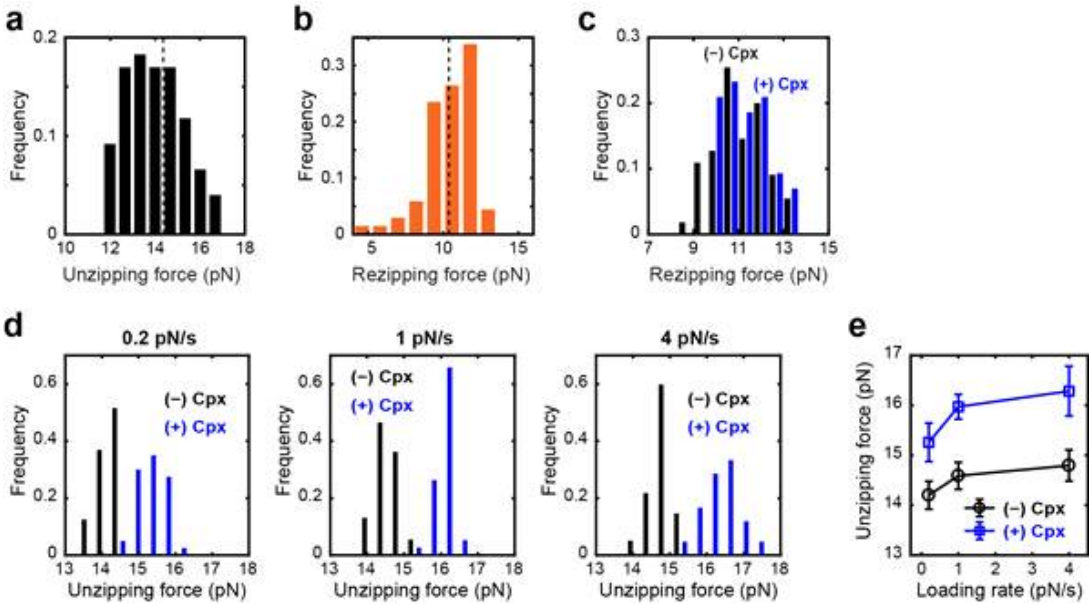

Supplementary Figure 4 Unzipping and rezipping forces of single SNARE complexes and the effect of complexin. (a,b) Distribution of SNARE unzipping (a; N = 96) and rezipping (b; N = 90) force (without Cpx) over multiple magnetic beads. The global unzipping and rezipping force (dashed lines) were 14.4 ± 1.3 and 10.4 ± 1.6 pN, respectively. The unzipping or rezipping forces in each bead were measured at least 5 times and averaged. (c) Distribution of rezipping force measured with a single magnetic bead without (black) and with (blue) 5 mM Cpx. (d,e) Loading rate dependence of unzipping force measured at 0.2, 1, and 4 pN/s, summarized in e. The error bars in e represent the standard deviations of the distributions in d.

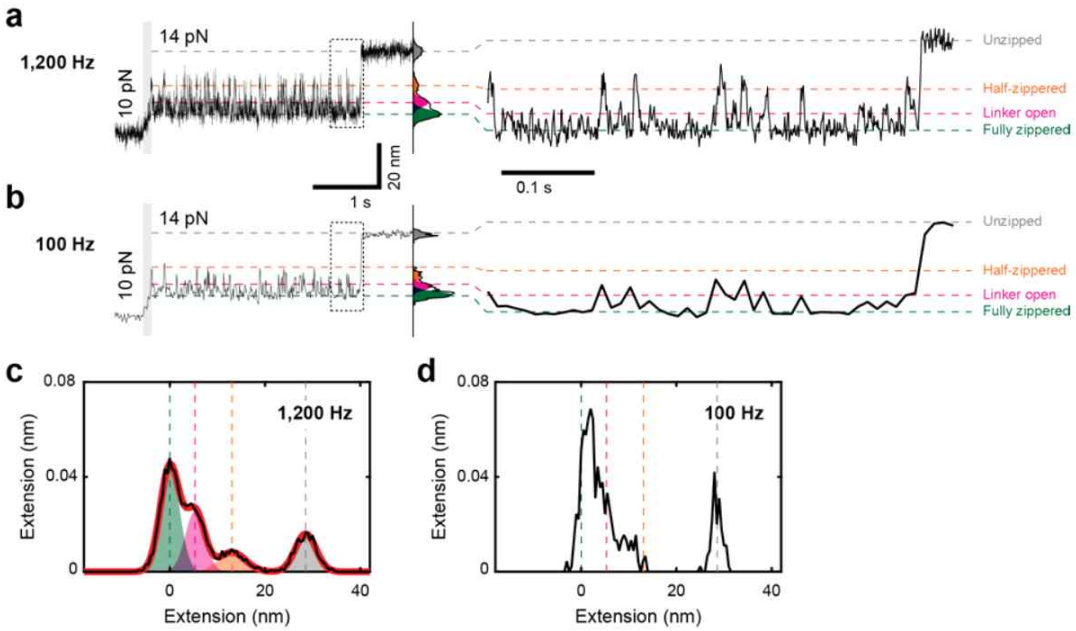

Supplementary Figure 5 Comparison of temporal resolutions for monitoring extensions of SNARE complexes. (a,b) Time traces for SNARE complex extension sampled at 1,200 Hz (a) and 100 Hz (b) in the absence of Cpx. (c,d) The corresponding distributions of extensions for the traces presented in a and b, respectively. Black lines represent the measured distributions. Dashed lines indicate the locations of the identified Gaussian components. Red line in c represents a fit to a Gaussian mixture model. The state locations in d are borrowed from c for comparison

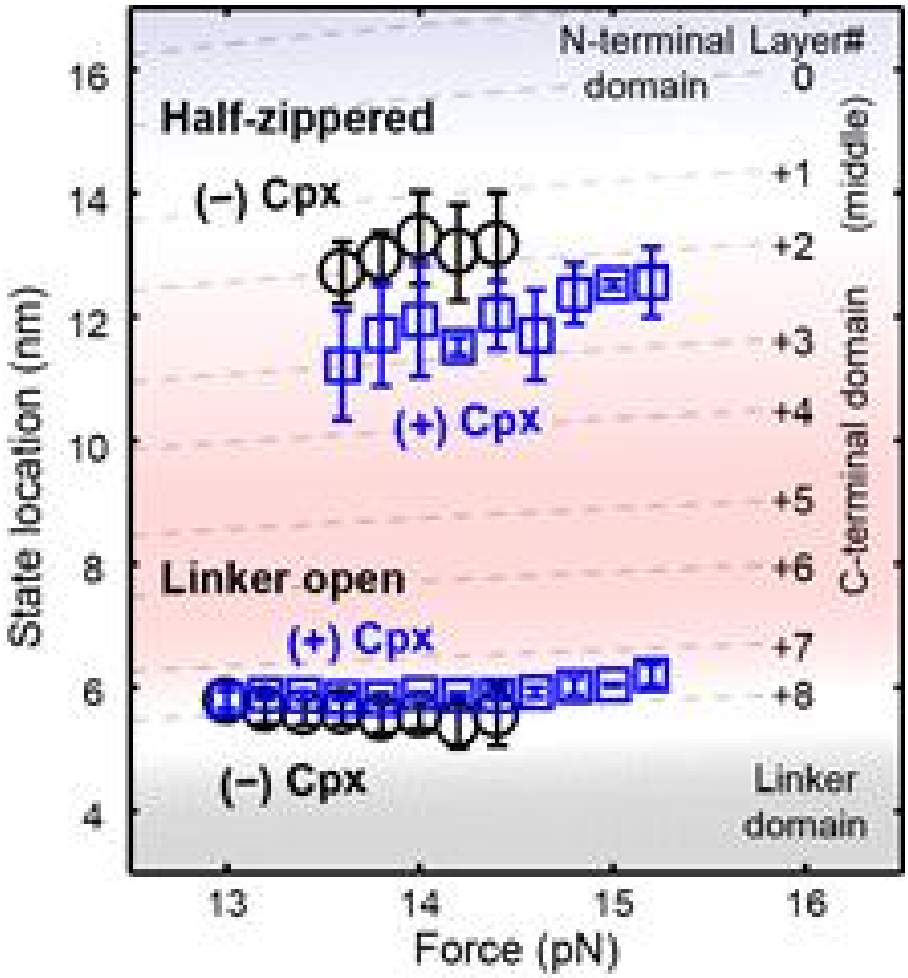

Supplementary Figure 6 Force-dependent changes in the location of linker-open (lower) and half-zippered state (upper) in the absence (black) and presence (blue) of Cpx. Dashed lines indicate the calculated distances of unzipping from the fully zippered state to the specified leucine zipper layers (Supplementary Note 2).

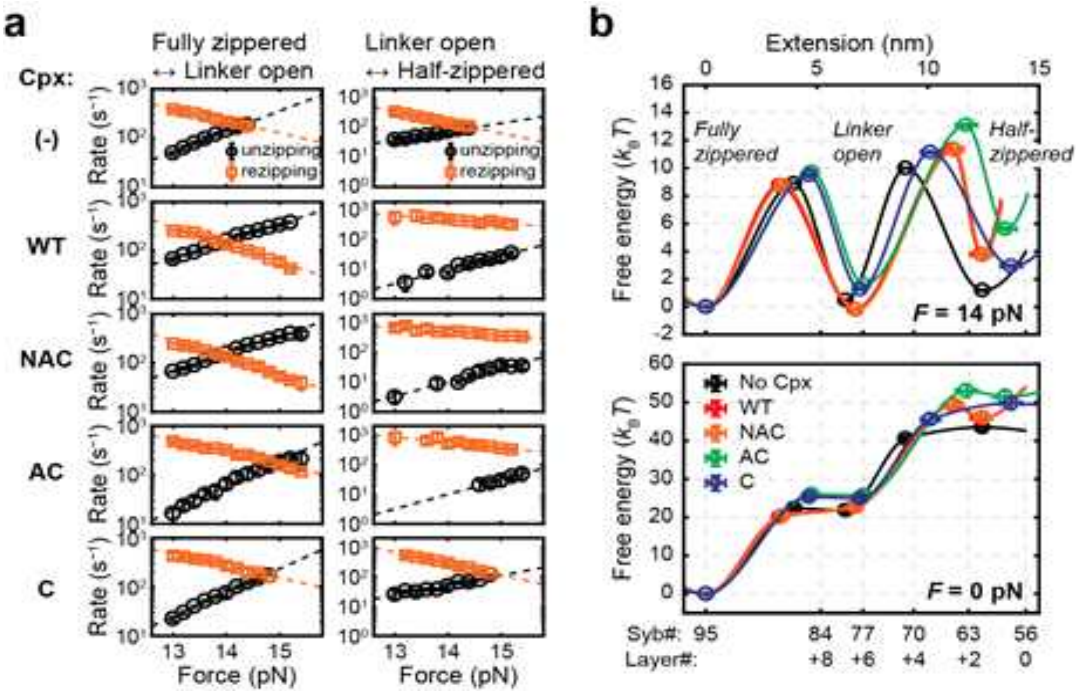

Supplementary Figure 7 Kinetic analysis of the zippered intermediates using hidden Markov modelling. (a) Linker-opening rates in the low-force regime. The data in Fig. 4e were fit to linear models and extrapolated to 0 pN. The intercepts at 0 pN were 2×10−4 s−1 without Cpx (black) and 2×10−4 s−1 with 5 μM Cpx (blue). (b) Force dependences of the transition rates between the zippered-state intermediates obtained from the modelled paths (such as in Fig. 4a in the main text) in the presence of the indicated Cpx variants. Dashed lines represent the fits to the Bell equation. (c) Energy diagrams for the three zippered states of SNARE complex at 14 (upper) and 0 pN (lower). The corresponding residue numbers of synaptobrevin-2 to which the SNARE complex is unzipped are indicated at the bottom.

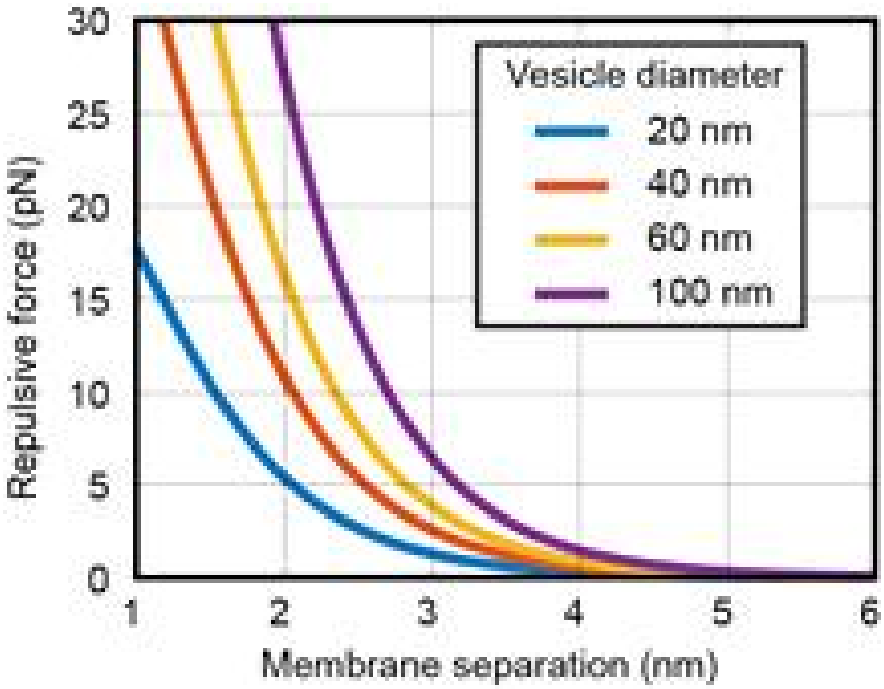

Supplementary Figure 8 Estimation of the repulsive force between a synaptic vesicle and the plasma membrane. The repulsive forces were calculated as described in a literature7 for the specified vesicle diameters (40 - 60 nm being the physiological average) in the fixed- potential limit. In the estimation, the surface potentials of vesicle and plasma membrane were assumed −25 and −70 mV, respectively, and the Debye screening length of 0.67 nm was used.

State	x (nm)	G_0 (k_BT)	$\Delta x^{\ddagger}_{unzip}$ (nm)	$\Delta G^{\ddagger}_{0,unzip}$ (k_BT)	$k_{0,unzip}$ (10^{-4} s^{-1})	$\Delta x^{\ddagger}_{rezip}$ (nm)	$\Delta G^{\ddagger}_{0,rezip}$ (k_BT)	$k_{0,rezip}$ (10^{5} s^{-1})
Fully zippered	0 (def.) 0 (def.)	0 (def.) 0 (def.)	3.9 ± 0.2 3.3 ± 0.1	22.3 ± 0.6 20.0 ± 0.4	2 ± 1 20 ± 8	N.A.	N.A.	N.A.
Linker-open	6.3 ± 0.2 6.7 ± 0.2	21.8 ± 0.7 22.6 ± 0.6	2.70 ± 0.07 4.4 ± 0.4	18.7 ± 0.2 27 ± 1	75 ± 20 0.03 ± 0.04	−2.3 ± 0.1 −3.4 ± 0.1	0.5 ± 0.3 −2.6 ± 0.5	6 ± 2 140 ± 60
Half-zippered	12.4 ± 0.3 12.4 ± 0.5	43.5 ± 0.8 46 ± 2	N.D.	N.D.	N.D.	−3.5 ± 0.1 −1.2 ± 0.2	−3.0 ± 0.4 3.3 ± 0.6	190 ± 80 0.4 ± 0.2

Supplementary Table 1 Sample assembly procedure for magnetic tweezers experiments. a SNARE–DNA conjugate was mixed with a 10-fold excess of NeutrAvidin for 30 min in advance. b Concentration with regard to the biotinylated end. c This step ensures the covalent coupling of the N-terminal ends of synaptobrevin-2 and syntaxin-1A. d The polystyrene beads serve as fiducial markers in tracking magnetic beads. e Surface coating of magnetic beads with anti-digoxigenin was carried out following manufacturer's protocol (Thermo Fisher).

State	x (nm)	G_0 (k_BT)	$\Delta x^{\ddagger}_{unzip}$ (nm)	$\Delta G^{\ddagger}_{0,unzip}$ (k_BT)	$k_{0,unzip}$ (10^{-4} s^{-1})	$\Delta x^{\ddagger}_{rezip}$ (nm)	$\Delta G^{\ddagger}_{0,rezip}$ (k_BT)	$k_{0,rezip}$ (10^{5} s^{-1})
Fully zippered	0 (def.) 0 (def.)	0 (def.) 0 (def.)	3.9 ± 0.2 3.3 ± 0.1	22.3 ± 0.6 20.0 ± 0.4	2 ± 1 20 ± 8	N.A.	N.A.	N.A.
Linker-open	6.3 ± 0.2 6.7 ± 0.2	21.8 ± 0.7 22.6 ± 0.6	2.70 ± 0.07 4.4 ± 0.4	18.7 ± 0.2 27 ± 1	75 ± 20 0.03 ± 0.04	−2.3 ± 0.1 −3.4 ± 0.1	0.5 ± 0.3 −2.6 ± 0.5	6 ± 2 140 ± 60
Half-zippered	12.4 ± 0.3 12.4 ± 0.5	43.5 ± 0.8 46 ± 2	N.D.	N.D.	N.D.	−3.5 ± 0.1 −1.2 ± 0.2	−3.0 ± 0.4 3.3 ± 0.6	190 ± 80 0.4 ± 0.2

Supplementary Table 2 Kinetic and thermodynamic parameters for the three zippered states. Kinetic parameters without (black) or with (blue) 5 mM WT Cpx.